







Au₄Mn: A localized ferromagnet with strong spin-orbit coupling, long-range ferromagnetic exchange, and high Curie temperature

Yangkun He ^{1,2,*}, Zsolt Gercsi,¹ Rui Zhang ¹, Yu Kang,² Yurii Skourski,³ Lucy Prendeville ¹, Orrie Larmour ¹, Jean Besbas ¹, Claudia Felser ², Plamen Stamenov,¹ and J. M. D. Coey¹

¹*School of Physics and CRANN, Trinity College, Dublin 2, Ireland*

²*Max-Planck-Institute for Chemical Physics of Solids, 01187 Dresden, Germany*

³*Dresden High Magnetic Field Laboratory (HLD-EMFL), Helmholtz-zentrum Dresden-Rossendorf, Dresden 01328, Germany*



(Received 9 August 2022; revised 11 October 2022; accepted 6 December 2022; published 13 December 2022)

Metallic Mn-based alloys with a nearest-neighbor Mn-Mn distance greater than 0.4 nm exhibit large, well-localized magnetic moments. Here we investigate the magnetism of tetragonal Au₄Mn with a Curie temperature of 385 K, where manganese has a spin moment of 4.1 μ_B and its orbital moment is quenched. Since 80% of the atoms are gold, the spin-orbit interaction is strong and Au₄Mn exhibits uniaxial magnetocrystalline anisotropy with surface maze domains at room temperature. The magnetic hardness parameter of 1.0 is sufficient to maintain the magnetization along the *c* axis for a sample of any shape. Au also reduces the spin moment of Mn through *5d-3d* orbital hybridization. An induced moment of 0.05 μ_B was found on Au under a pulsed field of 40 T. Density functional theory calculations indicate that the Mn-Mn exchange is mediated by spin-polarized gold *5d* and *6p* electrons. The distance dependence shows that it is ferromagnetic or zero for the first ten shells of Mn neighbors out to 1.041 nm (64 atoms), and very weak and oscillatory thereafter.

DOI: [10.1103/PhysRevB.106.214414](https://doi.org/10.1103/PhysRevB.106.214414)

I. INTRODUCTION

The magnetism of Mn depends critically on the interatomic manganese distance, giving a rich variety of possible magnetic structures. Generally, manganese has no magnetic moment for the shortest Mn-Mn distances ($d < 0.24$ nm), then a moment develops and the exchange coupling is antiferromagnetic for more typical nearest-neighbor separations (0.25 nm $< d < 0.28$ nm); bigger atomic moments and ferromagnetic coupling is found at longer separations ($d > 0.29$ nm) [1]. Although the general rule of ferromagnetism of Mn in ordered alloys with long Mn-Mn distances is known, the type of exchange interaction and magnetism (localized or itinerant) is not clear. For instance, dilute alloys such as **CuMn** with the largest Mn-Mn separations are spin glasses.

Au₄Mn crystallizes in Ni₄Mo-type tetragonal *I4/m* structure with Au occupying *8h* sites (0.2, 0.4, 0) and Mn on *2a* sites (0, 0, 0) [2] as shown in Fig. 1(a). Each Mn atom has 12 Au neighbors at almost the same distance of ~ 0.287 nm. Each Mn aligns with its two Mn nearest neighbors (1st NN) in chains along the *c* axis (d is 0.404 nm) and there are eight next-nearest neighbors (2nd NN) at 0.5 nm in the four surrounding chains, which also couple ferromagnetically. Localized manganese moments of $\sim 4.1 \mu_B$ that couple

ferromagnetically along the *c* axis were reported in early work [2]. The material is prototypical to study the magnetism of Mn at large Mn-Mn separations. What makes this material also interesting is its high Curie temperature T_C (~ 380 K) [3] in an almost dilute system with only 20 at. % Mn. In addition, in the Au₄*X* structure, *X* can be either an early *3d* transition element or a late *4f* element [4]. Thus, it is a rare example of a system where the magnetism of *3d* and *4f* elements can be compared in the same crystal field environment.

In light of the above, the magnetism of Au₄Mn raises some questions that we address in this paper: (1) Is the magnetocrystalline anisotropy uniaxial and strong enough to resist the demagnetizing field for a sample of any shape? What is the domain structure? (2) What is the influence of spin-orbit coupling? Is the orbital moment of Mn quenched, or does it contribute to the total moment as in a rare earth? (3) What is the nature of the exchange interactions *J*, direct or Ruderman-Kittel-Kasuya-Yosida (RKKY)? (4) What does the band structure look like? Is Au magnetic in Au₄Mn? Here we address these questions experimentally, and compare the results with density functional theory calculations for Au₄Mn.

II. METHODS

High-purity Au and Mn were mixed in an Al₂O₃ crucible before sealing them in a quartz tube under Ar. The tube was heated at 1100 °C for one day for homogeneity. It was then slowly cooled to 350 °C over five days, followed by a three-week anneal to improve the atomic order of the polycrystalline material. The crystal structure was characterized by x-ray diffraction (XRD). Magnetization was measured in a superconducting quantum interference device magnetometer

*heyay@tcd.ie

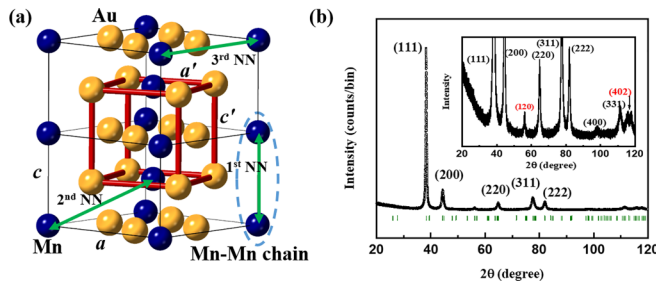


FIG. 1. (a) Crystal structure of Au_4Mn (black unit cell showing a double cell along c axis) as a distorted fcc structure (red cell). Blue and yellow atoms are Mn and Au respectively. The first-nearest-neighbor (1st NN) to third-nearest-neighbor (3rd NN) Mn pairs are shown. (b) XRD pattern of Au_4Mn . The Bragg peak positions are shown by green vertical bars. The indices shown are based on the fcc structure. The inset shows the enlarged XRD pattern.

(SQUID, Quantum Design). High-field magnetization measurements were performed in the Dresden High Magnetic Field Laboratory in pulsed fields of up to 56 T. The magnetic domain images were observed by a magneto-optical Kerr microscope (Evico Magnetics) at room temperature on a polished surface. A rare-earth iron garnet film (with saturation field 0.8 mT) was used to reveal the stray field at the surface. Ferromagnetic resonance (FMR) measurements were performed using a Bruker EMX electron paramagnetic resonance (EPR) spectrometer with an X-band bridge operating at 9.614 GHz on a platelike sample with the field perpendicular to the plane. The static magnetic field was ramped from 0 to 0.6 T and the field derivative of the absorbed microwave power was measured as a function of the magnetic field. *Ab initio* calculations based on density functional theory (DFT) were carried out using norm-conserving pseudopotentials and pseudoatomic localized basis functions implemented in the OPENMX software package [5]. The generalized gradient approximation Perdew-Burke-Ernzerhof (GGA-PBE) [6] was used for all the calculations. The structure was fully relaxed to minimize interatomic forces. We used a ten-atom superstructure with eight Au and two Mn atoms with $(11 \times 11 \times 15)$ k points to evaluate the total energies. This extended structure also allowed us to simulate the electronic structure with both ferromagnetic (FM) and antiferromagnetic (AFM) couplings of the manganese. Pregenerated fully relativistic pseudopotentials and the pseudoatomic orbitals with a cutoff radius of 6 atomic units (a.u.) were used with $s3p3d3$ for Mn and 7 a.u. with $s3p3d3f1$ for Au. An energy cutoff of 300 Ry was used for the numerical integrations. The convergence criterion for the energy minimization procedure was set to 10^{-8} hartree. The spin-orbit interaction (SOI) was turned on for the calculations. The magnetocrystalline anisotropy (MAE) was calculated using a 5-atom cell and a large number of k points $(15 \times 15 \times 19)$ for high precision.

III. RESULTS

A. Crystal structure

The crystal structure was characterized by x-ray diffraction (XRD) on polycrystalline material. The total time for

the XRD is 56 h. Since Au_4Mn is not brittle, we were unable to make strain-free powders for the diffraction experiment. We used a polished bulk sample and there may be some texture that could influence the relative intensities of the reflections. The crystal structure and the corresponding XRD pattern are shown in Fig. 1. The fitted lattice constants in the Ni_4Mo -type tetragonal $I4/m$ structure are $a = 0.6459(8)$ nm and $c = 0.4042(3)$ nm. The crystal has a tetragonally distorted face-centered-cubic structure [2], where the lattice constants are $a' = \sqrt{2/5} a = 0.4085(5)$ nm and $c' = c = 0.4042(3)$ nm, as shown in Fig. 1(a). c' is slightly smaller than a' ($c'/a' = 0.99$) because of a contraction along the $[001]$ Mn chains. Atomic ordering was confirmed by the superlattice (120) peak and the splitting of the fcc (402) peak.

B. Magnetic properties

The magnetization curves at different temperatures are shown in Fig. 2(a). The extrapolated spontaneous moment m_s in zero field measured at 4 K is $4.1 \mu_B/\text{f.u.}$, which decreases to $2.8 \mu_B/\text{f.u.}$ at room temperature. The high field slope of the magnetization curve at 4 K is quite steep, $0.02 \mu_B/\text{T}$, which is similar to that of ferromagnetic Au_4V with the same structure [7]. This slope is accompanied by a large volume magnetostriction [8]. The high field magnetization data shown in Fig. 2(b) saturates at 40 T with a moment $m = 4.5 \pm 0.1 \mu_B/\text{f.u.}$ The additional moment of $0.4 \mu_B$ induced by the high magnetic field is similar to that of Au_4V [7]. The spontaneous moment as a function of temperature is plotted in Fig. 2(c). Mean field theory was used to fit the curve with $S = 2$ (S is the spin quantum number), which matches the experiment. The paramagnetic Curie temperature θ_p fitted by the mean field model is 387 K. The inverse susceptibility χ^{-1} as a function of temperature is plotted in Fig. 2(d), indicating an effective magnetic moment m_{eff} of $4.9 \mu_B$, in agreement with a previous report [9], and a localized moment with $S = 2$.

The magnetocrystalline anisotropy was determined by the anisotropy field deduced from ferromagnetic resonance (FMR) at room temperature as shown in Fig. 2(e). For an isotropic free electron, the frequency of 9.614 GHz corresponds to a remanence $\mu_0 H_R = 0.343$ T. In our polycrystalline sample the total signal comes from a distribution of crystallites with slightly different resonance frequencies. Each frequency is determined by the direction of the applied field θ (the angle between the magnetic field and easy axis), the crystallite magnetization, and its magnetocrystalline anisotropy. The number of the crystallites participating in the resonance is largest at the fields where $dH_R/d\theta = 0$. The angular dependence of the resonant field shows that the low field FMR position corresponds to the case when the applied field is parallel or close to the easy axis of the crystals in the polycrystalline sample; the high field position indicates the field is nearly in the ab plane [10,11]. For the low field FMR position, if we ignore the high-order anisotropy terms, the relationship between the FMR field position $\mu_0 H_R$, anisotropy field $2K/M_s$, and the angular frequency of the microwave field

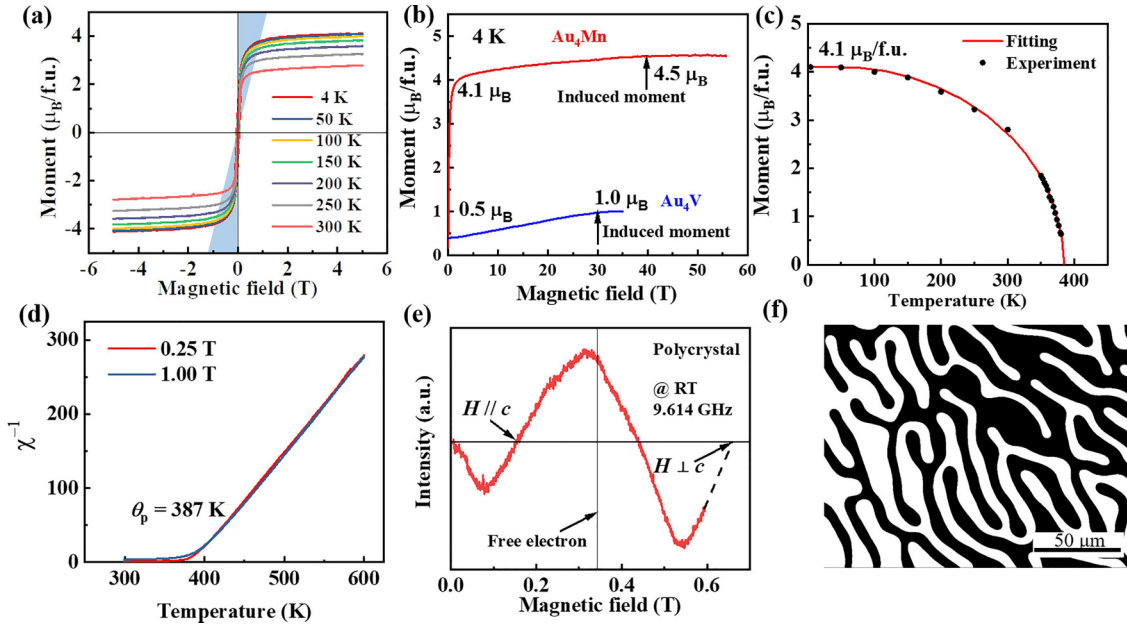


FIG. 2. Magnetic properties. (a) Magnetization curves at different temperatures. The multidomain state exists under a small magnetic field (blue region). (b) Magnetization measured in a pulsed magnetic field of 56 T at 4 K. The saturation was found at 40 T (see the cross of two dashed lines). The data for Au₄V are from Ref. [7]. (c) Saturation magnetization as a function of temperature and the $S = 2$ fit by mean-field theory. The data below 300 K were obtained from the M - H curves; the data close to the T_C were measured under an applied magnetic field of 0.25 T. (d) Inverse susceptibility χ^{-1} measured under 0.25 and 1 T. (e) FMR spectrum at room temperature (RT) for the derivative of the polycrystals of micrometer size. Crystals with their easy axis closer to the field direction exhibit smaller $\mu_0 H_R$ while larger magnetic field is required for crystals with the c axis perpendicular to the field. (f) Magnetic domain structure at room temperature.

ω satisfies [10]

$$\left(\frac{\omega}{\gamma}\right)^2 = \left(\mu_0 H_R + \mu_0 M(N_x - N_z) + \frac{2K_1}{M_s}\right) \times \left(\mu_0 H_R + \mu_0 M(N_y - N_z) + \frac{2K_1}{M_s}\right), \quad (1)$$

where γ is the gyromagnetic ratio of 28 GHz T^{-1} and N_x , N_y , and N_z are the demagnetizing factors along different directions. For our platelike sample with the field perpendicular to the plane, $N_x = N_y = 0$ and $N_z = 1$. Using Eq. (1), the anisotropy field $2K_1/\mu_0 M_s$ at room temperature is roughly estimated as 0.76 T. The corresponding value of K_1 is $100 \pm 10 \text{ kJ m}^{-3}$, which agrees with a previous torque measurement [2]. The magnetic hardness parameter $\kappa = \sqrt{K_1}/(\mu_0 M_s^2)$, a convenient figure of merit for permanent magnets [12], is 1.0. At low temperature K_1 increases to 300 kJ m^{-3} [2], while κ retains the same value. This means Au₄Mn is a highly anisotropic material, which can maintain the perpendicular anisotropy in any shape below T_C .

The magnetic domain structure was observed on a polished surface after demagnetization by an AC magnetic field, as shown in Fig. 2(f). Maze surface domains, a sign of strong uniaxial anisotropy, were observed, similar to those in many hard magnetic materials such as Nd₂Fe₁₄B [13], MnBi [14], and Rh₂CoSb [15]. This confirms the large magnetocrystalline anisotropy from the FMR measurement. Note that the Kerr rotation angle in our magneto-optical measurement is lower than the resolution limit ($< 0.01^\circ$) using red (1.96 eV) or blue (3.06 eV) light different from the predicted value of $\sim 0.4^\circ$ [16], therefore a rare-earth iron garnet film (the saturation field

is 0.8 mT) was needed to reveal the stray field and domain structure at the surface.

C. Band structure

In order to reveal the nature of the exchange interaction and the origin of high T_C in Au₄Mn, first principles calculations were used to investigate the band structure. Our calculation shows a band structure similar to that of a previous study, which discussed the role of Au on magnetism in metallic systems [17]. Figure 3(a) shows the total (TDOS) and partial (PDOS) densities of states in Au₄Mn. The occupied spin channels in TDOS are symmetrical up to about $E_F - 2 \text{ eV}$, where the $3d$ bands of Mn split by on-site exchange dominate for the spin up channel. The unoccupied minority Mn $3d$ bands are located about 1.5 eV above Fermi level. The magnetic Mn-Mn coupling is strongly ferromagnetic, and with about 20 meV/atom lower in energy as compared to an antiferromagnetic spin alignment. The symmetric spin channels of PDOS for Au suggest a small contribution to the total magnetic moment. The calculated net moment of Au is small, $0.05 \mu_B$ per atom, in agreement with previous x-ray magnetic circular dichroism (XMCD) measurements [18,19]. The orbital-specific DOS of Mn is shown in Fig. 3(b). The contribution to the DOS from $3d$ bands at the Fermi level is small [0.35 eV^{-1} in the spin down channel shown in Fig. 3(c)] compared to 1 – 2 eV^{-1} for transition metals Fe, Co, and Ni] and free electrons of Au are dominant instead, resulting in a small electronic specific heat of $\gamma = 2 \text{ mJ/mole K}^2$ [20] and a tiny Kerr rotation angle with visible light.

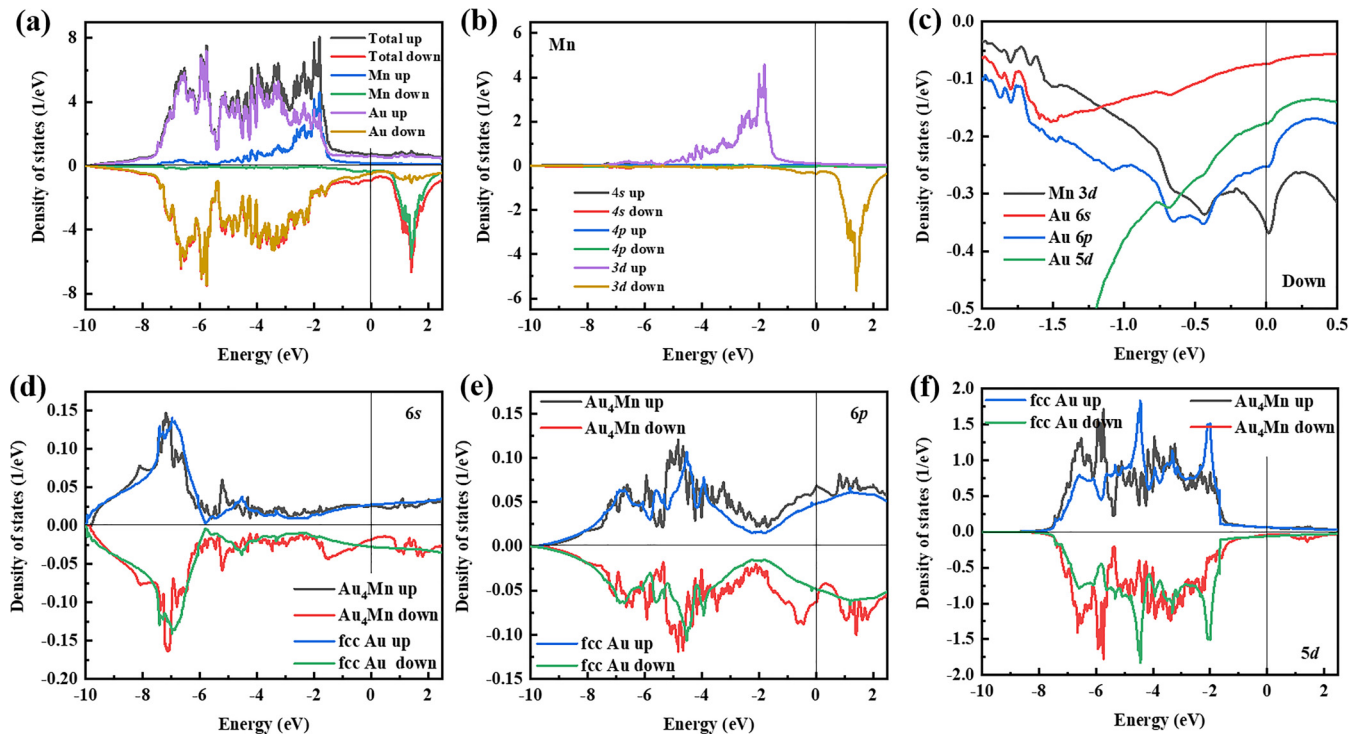


FIG. 3. Results of first principles calculations. (a) Partial DOS of Au and Mn in Au₄Mn together with total DOS. (b) DOS of Mn 3*d*, 4*s*, and 4*p* orbitals in Au₄Mn. (c) DOS close to the Fermi level in the spin down channel. (d)–(f) Comparison of the DOS of Au 6*s*, 6*p*, and 5*d* orbitals in pure Au and Au₄Mn.

We compare the DOS of Au 6*s*, 6*p*, and 5*d* orbitals in pure fcc Au and Au₄Mn in Figs. 3(d)–3(f). There is little difference in 6*s* and 6*p* orbital occupations in the spin up channel, but a significant difference is found in the spin down channel close to the Fermi level, which means that the 6*s* and 6*p* electrons in Au₄Mn are polarized by Mn due to band hybridization. In particular, DOS of Au 6*p* orbitals shows strong resemblance to Mn 3*d* orbitals close to the Fermi level as shown in Fig. 3(c), indicating its important role in the exchange and the related magnetism of Au₄Mn (discussed below). In Au₄Mn, the Au 5*d* bands are symmetric and nearly fully occupied, where the top of the bands is about 2 eV below the Fermi level. A slight shift in Au 5*d* orbital occupation can be observed due to hybridization with the overlapping majority spin bands of 3*d* Mn when compared to pure fcc Au.

To further study the influence of the band hybridization on the magnetism, we have calculated the electronic structure of pure Mn in Au₄Mn lattice after removing the Au atoms in a hypothetical body-centered-tetragonal (bct) structure. In hypothetical “bct Mn,” the exchange splitting is larger with spin up channel 4 eV below E_f and the moment is a good quantum number of 5.0 μ_B per Mn, larger than the 4.1 μ_B in Au₄Mn with a 3*d*-5*d* hybridization.

IV. DISCUSSION

A. Localized moments

The series Au₄X ($X = \text{Sc, Ti, V, Cr, Mn, Er, Tm, Yb, Lu}$) offers a way to compare the magnetism of 3*d* and 4*f* elements sharing the same crystal field environment. We summarize the magnetic properties of the series in Ta-

ble I. All these compounds exhibit matching moments from both inverse susceptibility and mean field theory, indicating a localized moment on X. The electronic specific heat of $\sim 2 \text{ mJ mol}^{-1} \text{ K}^{-2}$ [20] in Au₄Mn is much lower than in itinerant ferromagnets such as CoS₂ [21] and Ni [22], indicating a small density of states at the Fermi level from the broad *s*, *p* band. The tiny Kerr rotation angle in our optical measurement further indicates the absence of any highly spin-polarized band at the Fermi level, similar to Gd [23]. Unlike the rare earths, the orbital moments of the 3*d* elements are quenched.

B. Distance-dependent moments and exchange interactions

We compare in Fig. 4(a) the magnetic moment as a function of nearest-neighbor Mn-Mn distance for many ferromagnetic materials where Mn is the only magnetic element. These materials fall into two categories. A small distance of 0.28–0.30 nm leads to itinerant magnetism with direct exchange mechanism where the magnetic moment per Mn varies from 1.5 μ_B (in Mn₂VA1) to 4 μ_B (MnBi) [24]. Localized magnetism is often found in Mn-based magnets with larger Mn-Mn distances. Magnets where the distance is >0.4 nm, including many (half) Heusler alloys (and also Au₄Mn), all exhibit a moment of about 4 μ_B /Mn.

Strong direct exchange between Mn pairs can hardly occur in these compounds based on localized 3*d* states. Previous theoretical studies revealed the crucial role of indirect exchange coupling for the neighbor nonmagnetic elements in Heusler alloys with a large Mn-Mn distance [25–27]. Spin polarized *s*, *p* bands mediate interatomic covalent interactions between the Mn 3*d* states. In Au₄Mn, we have also found the

TABLE I. Magnetic properties of Au₄X (X = Sc, Ti, V, Cr, Mn, Er, Tm, Yb, Lu). The m_s and m_{eff} match well for a localized moment. Au₄Ti, Sc, Lu are nonmagnetic.

	m_s (μ_B) Experiment	m_{eff} (μ_B) Experiment	J (Total moment)		m_{eff} (μ_B) Theory	T_C/T_N (K)	Exchange Interaction	Ref.
Au ₄ Mn	4.1	4.9	S	2	4.9	387	FM	this work
Au ₄ Cr	3.2	4	S	3/2	3.9	380	AFM	[9]
Au ₄ V	1	1.7	S	1/2	1.7	57	FM	[7]
Au ₄ Ti	0	0	0	0	0			[3]
Au ₄ Sc	0	0	0	0	0			
Au ₄ Er		9.8	$L + S$	15/2	9.6	5	RKKY	[4]
Au ₄ Tm		7.6	$L + S$	6	7.6	2	RKKY	[4]
Au ₄ Yb		4.5	$L + S$	7/2	4.5	<6	RKKY	[4]
Au ₄ Lu	0	0	0	0	0			

similar spin polarized $6s$ and $6p$ states of Au shown in Fig. 3, so we might think a RKKY interaction is responsible for the ferromagnetism.

We have therefore calculated the interaction strength as a function of Mn-Mn distance d in Au₄Mn, shown in Fig. 4(b) where the points represent the successive shells of Mn neighbors, and $J_{\text{eff}} = ZJ$, where Z is the number of neighbors in a shell. The exchange fluctuates with distance, but there are no antiferromagnetic interactions for the first ten shells with $d \leq 1.041$ nm. The exchange interactions are all ferromagnetic or zero. Only beyond that, where there is little further net contribution to the coupling, is the exchange RKKY-like, oscillating in sign. The results are summarized in Table II.

The RKKY function $F(\xi) = (\sin \xi - \xi \cos \xi)/\xi^4$ is plotted in Fig. 4(c), where $\xi = 2k_F d$, k_F is the Fermi wave vector $k_F = (3\pi^2 n)^{1/3}$ for the free-electron gas, and n is the number of free electrons per unit volume [1]. In a simple model with one free electron per Au atom, $n = 4.74 \times 10^{28} \text{ m}^{-3}$ and $k_F = 1.12 \times 10^{10} \text{ m}^{-1}$, and $F(\xi)$ is the dashed curve. In our calculation we find a reduced number of 2.1 free electrons per formula unit due to hybridization of Au $6s$, $6p$ orbitals with Mn $3d$ orbitals, which corresponds to the solid curve. The first- and second-neighbor exchange is of opposite sign in the first case, favoring a spin structure of ferromagnetic chains coupled antiferromagnetically, as in Au₄Cr [28]. The calculated magnetic ordering temperature is much lower than the experimental one, assuming $J_{\text{sd}} = 0.36 \text{ eV}$ for Mn [29] in the RKKY model. In our DFT calculation, the Curie tempera-

ture is 460 K if Mn-Au $3d$ - $5d$ interactions are ignored, while it is only slightly less, 439 K, if all exchange interactions are considered.

We further compare with Mn-based dilute alloy spin glasses where the Mn-Mn distances are even larger and Kondo temperatures are only of order 10 mK. There the dominant exchange is also the s - d RKKY interaction. In fcc AuMn spin glass, a dilute alloy where a few percent of manganese impurities are dispersed in an fcc gold matrix, the effective manganese moment measured in the paramagnetic state is around $5.5 \mu_B$ [30]. With 1% manganese in this system, the average Mn-Mn distance is 1.19 nm and the spin freezing temperature $T_f < 20 \text{ K}$ [30]. At these distances, the electrons of Mn $3d$ shells cannot interact directly and exchange is RKKY via the oscillating spin polarization of the gold conduction band. It is equally likely to be ferromagnetic or antiferromagnetic due to the disorder.

The T_C for localized Mn-based magnets is sensitive to the distance or the number of Mn atoms per volume as shown in Fig. 4(d). When the Mn concentration (number of atoms per m^3) decreases slightly the T_C drops significantly, as shown from groups of materials with the same valence electrons including NiMnSb-PtMnSb [1], Rh₂MnGe-Rh₂MnSn-Rh₂MnPb [24], and Cu₂MnAl-Cu₂MnIn-Au₂MnAl [24]. This trend is opposite to itinerant magnets MnAs-MnSb-MnBi [1] where T_C increases with atomic distance. Au₄Mn is significantly off the trend for itinerant magnets. The T_C of Au₄Mn is sensitive to the lattice constant. With increasing pressure, both the M_s and T_C increase [31] due to the enhanced hybridization with smaller lattice parameters, therefore the magnetism of Au₄Mn thin films grown on piezoelectric substrates could easily be modified by strain.

The outstanding property of Au₄Mn compared to other $3d$ magnets with a similarly low concentration of magnetic atoms is its relatively high T_C . According to the mean field model, $T_C = 2ZJS(S+1)/3k_B$, where Z is the number of interacting neighbors, k_B is the Boltzmann constant, and J is the exchange constant. Taking $Z = 10$ (counting 1st NN and 2nd NN Mn) and $S = 2$, we find $J/k_B = 9.6 \text{ K}$. Usually itinerant Mn-based ferromagnets have a much larger J , due to the close Mn-Mn distance, and smaller moments as shown in Fig. 4(e). Other examples with long Mn-Mn distances and large local moments where J/k_B is around 10 K include Heusler $X_2\text{MnZ}$

TABLE II. Exchange Interactions in Au₄Mn by DFT calculation.

Shell number	Mn-Mn distance (nm)	Z	ZJ (meV)	Sum (meV)
1	0.404	2	1.8	8.5 (59%)
2	0.499	8	3.4	
3	0.645	4	3.3	
4	0.760	8	1.0	
5	0.762	8	1.3	
6	0.808	2	0.0	
7	0.912	4	1.3	
8	0.997	8	0.0	
9	1.034	8	1.1	
10	1.041	8	1.0	14.3 (100%)

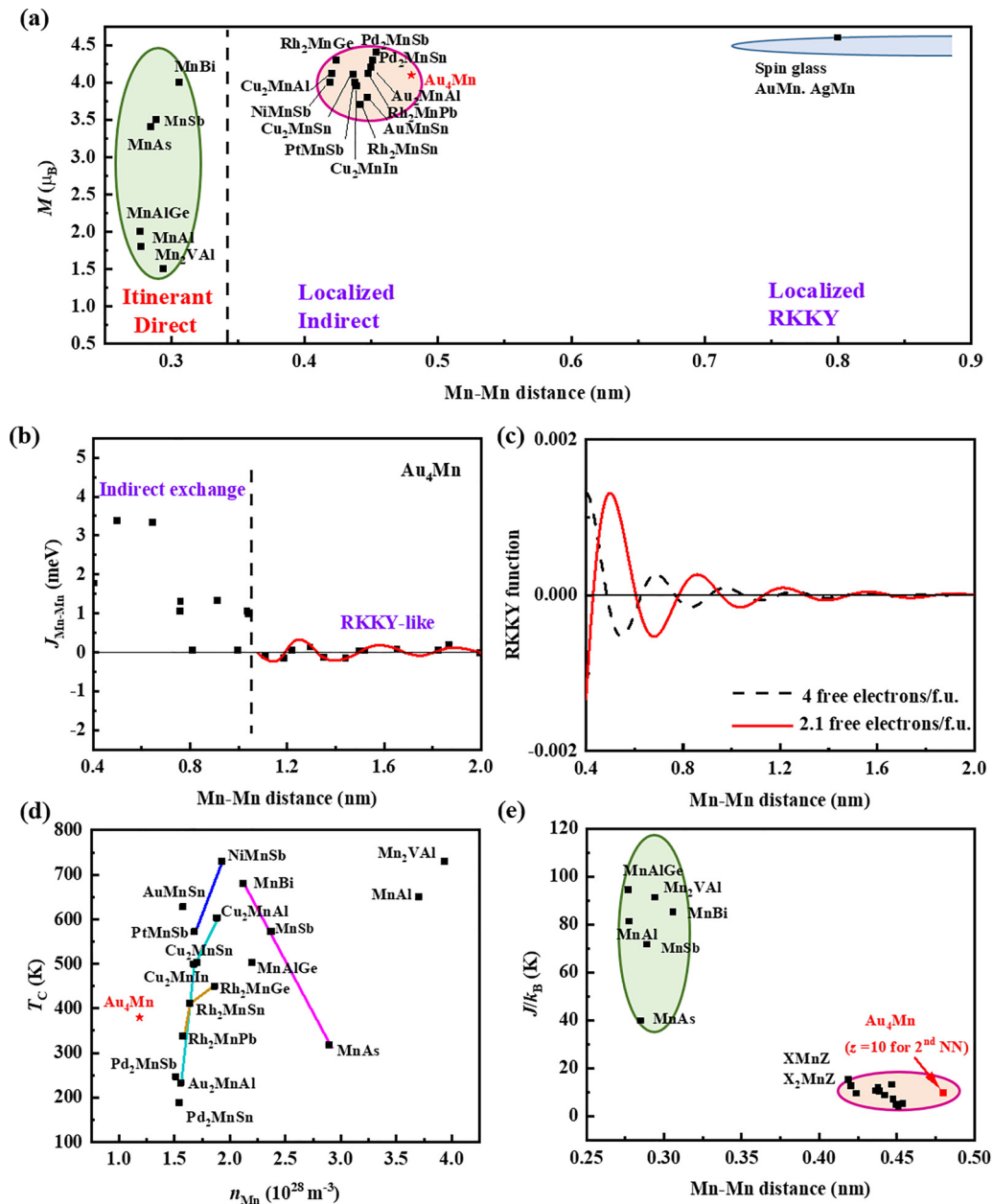


FIG. 4. (a) Magnetic moment versus Mn-Mn distance in Mn-based magnets. All materials are ferromagnets where Mn is the only magnetic element, except for the dilute Mn spin glasses, where the Mn moment is deduced from the effective moment in the paramagnetic state [30]. (b) Exchange interaction strength as a function of Mn-Mn distance in Au_4Mn . (c) Distance-dependent RKKY function with different free electron numbers. (d) The relationship between T_C and Mn concentration. Data are from Refs. [1,24,32–34]. (e) Exchange interaction constant J as a function of Mn-Mn distance in Mn-based alloys. XMnZ and X_2MnZ refer to Heusler and half Heusler alloys as also shown in the localized region in (a).

and half Heusler XMnZ materials with $Z = 12$. Others are shown in the localized region in Fig. 4(a). If we only account for the 1st NN Mn and take $Z = 2$, J/k_B is unreasonably large. Therefore both 1st NN and 2nd NN Mn-Mn interactions contribute to the ferromagnetism on Au_4Mn [28].

C. Spin-orbit coupling and high field magnetization

The spin-orbit coupling strength increases with the atomic number. Therefore, the value for Au is larger than most other common elements that can form ferromagnetic alloys [35].

High spin-orbit coupling causes high anisotropy, therefore the gold host significantly enhances the anisotropy.

We now consider possible reasons for the magnetization behavior in high fields. The anisotropy energy K_1 is 300 kJ m^{-3} at low temperature from torque measurements [2] or 500 kJ m^{-3} from our DFT simulations, corresponding to an anisotropy field $2K_1/M_s$ of 1.3–2.1 T. This is significantly smaller than the field of more than 40 T applied in the pulsed field measurement. Therefore, the increase of the moment at high field is not related to a moment that is unsaturated because of polycrystalline magnetocrystalline anisotropy.

The dimensionless high-field susceptibility χ of Au₄Mn is of order 10^{-3} (SI), two orders larger than the Pauli susceptibility (10^{-5}) and also much larger than that of a ferromagnet such as Fe with $\chi = 3.8 \times 10^{-4}$ [36]. This large χ is similar to that of Rh₂CoSb, 1×10^{-3} [15], where there is an induced moment $0.3 \mu_B$ of Rh due to the $3d$ - $4d$ hybridization. Therefore, the high field slope in Au₄Mn should have a different origin from simple Pauli susceptibility. It is likely to relate to progressive field-induced flipping of a small moment of Au due to the hybridization Mn and Au d orbitals. However, the first possibility to consider is some manganese disorder that introduces Mn-Mn nearest-neighbor pairs on adjacent sites that couple antiferromagnetically. This results in a decreased net moment and T_C [37]. The additional $0.4 \mu_B/\text{f.u.}$ under high magnetic field could be attributed to at least 5% of misplaced Mn whose moment flips under magnetic field. We cannot fully rule out some manganese disorder, but it does not explain why a similar phenomenon is observed in the vanadium compound [7]. Such Mn disorder would reduce the Curie temperature, but our samples actually have slightly higher T_C than previously reported [3].

The second possibility is long-range helical or spiral spin structure of Mn. The period would lengthen and the magnetization would eventually saturate in high field. However, neutron diffraction has shown that Au₄Mn is a simple ferromagnet [3], and we could find no more stable noncollinear spin structure in our calculation. Again, there is no reason why the vanadium alloy should saturate in the same field.

A third thought, ruled out by the small density of states calculated at the Fermi level, is that Mn atoms increase their moment significantly under applied magnetic field in a paraprocess. The manganese moment does depend on the tetragonal distortion, which is larger at low temperature, as indicated by the anisotropic thermal expansion [38], but our calculation shows that the lattice constant would have to change by much more than 10% to increase the moment from $4.1 \mu_B/\text{f.u.}$ to $4.5 \mu_B/\text{f.u.}$

Last, we return to the magnetism of Au. Usually the $5d$ orbitals of Au are fully occupied and the electrons are unpolarized, so Au is nonmagnetic. But when hybridized with Mn, a small spin moment is induced, which might be field dependent, like that in the enhanced Pauli paramagnet YCo₂ [39]. In fact, an induced spin moment of $0.016 \mu_B$ and $0.035 \mu_B$ per Au was observed by XMCD under 3 and 6 T, respectively [18,19], which agrees with our high-field slope of $0.02 \mu_B/\text{T}$ in Figs. 2(a) and 2(b) in this field range. It is also possible that the spin moment on Au rotates continuously from antiparallel

to parallel to the manganese moments under applied magnetic field. If, in the ground state, the moments of Au and Mn are antiparallel, flipping a net moment of $0.05 \mu_B/\text{Au}$ could explain the experimental result ($0.05 \times 4 \times 2 = 0.4 \mu_B/\text{f.u.}$). A similar argument can be made for the vanadium compound. It seems that the gold in Au₄Mn should be regarded as magnetic gold to some degree.

V. CONCLUSION

From our study of the magnetism of ferromagnetic Au₄Mn, we find that the large, localized manganese moment and significant ferromagnetic exchange coupling at Mn-Mn separations up to 1.04 nm are related to indirect exchange mediated principally by Au $6p$ electrons. Evidence comes from the well-matched values of m_s and m_{eff} , the small Kerr rotation angle and the band structure calculations. The manganese orbital moment is quenched, as in most $3d$ magnets. The high T_C is a result of the large, localized manganese moments and ferromagnetic exchange in the first ten nearest-neighbor shells. Since 80% of its atoms are heavy element Au with a strong spin-orbit coupling, its $5d$ orbital is hybridized with Mn $3d$ and aligned under high magnetic field. There is a moment of $0.4 \mu_B/\text{f.u.}$ on the gold under a magnetic field of 40 T. This hybridization also reduces the Mn moment from an ideal of $5.0 \mu_B$ to $\sim 4.1 \mu_B$. The uniaxial magnetocrystalline anisotropy at room temperature is manifested by maze surface domains. The magnetic hardness parameter of 1.0 is sufficient to maintain the c -axis anisotropy in any shape. We summarized the distance-dependent magnetism of Mn by comparing Au₄Mn with many reported Mn-based materials, and find that (1) a small interatomic distance of 0.28–0.30 nm leads to itinerant ferromagnetism where the magnetic moment can vary greatly; (2) localized magnetism with indirect exchange interactions is found in Mn-based magnets with Mn-Mn distances >0.4 nm, which exhibit a Mn moment of about $4 \mu_B$.

ACKNOWLEDGMENTS

This work was supported by Science Foundation Ireland, under the MANIAC, SFI-NSF China Project No. 17/NSFC/5294 and ZEMS Project No. 16/IA/4534. We acknowledge the support of the Dresden High Magnetic Field Laboratory (HLD) at HZDR and members of the European Magnetic Field Laboratory (EMFL).

-
- [1] J. M. D. Coey, *Magnetism and Magnetic Materials* (Cambridge University Press, Cambridge, UK, 2010).
 - [2] K. Adachi, T. Ido, and K. Sato, Temperature Dependence of magnetocrystalline anisotropy of ordered Au₄Mn, *Trans. Jpn. Inst. Met.* **18**, 299 (1977).
 - [3] R. S. Toth, A. Arrott, S. S. Shinozaki, S. A. Werner, and H. Sato, Studies of Au₄X-ordered alloys: Electron and neutron diffraction, resistivity and specific heat, *J. Appl. Phys.* **40**, 1373 (1969).
 - [4] L. R. Sill, W. J. Mass, A. J. Fedro, J. C. Shaffer, and C. W. Kimball, Magnetic properties of the system Au₄R (R = Er, Tm, and Yb), *J. Appl. Phys.* **42**, 1297 (1971).
 - [5] See <http://www.openmx-square.org>.
 - [6] J. P. Perdew, K. Burke, and M. Ernzerhof, Generalized Gradient Approximation Made Simple, *Phys. Rev. Lett.* **77**, 3865 (1996).
 - [7] G. Kido, N. Miura, M. Matsui, and K. Adachi, Magnetization process in Au₄V single crystal under pulsed high magnetic fields, *J. Magn. Magn. Mater.* **31**, 283 (1983).

- [8] K. Kondo, Estimation of the pressure effect of the absolute saturation magnetization of Au₄Mn, indium heusler alloy and MnSb by forced magnetostriction measurement, *J. Phys. Soc. Jpn.* **40**, 411 (1976).
- [9] H. Sato, M. Yessik, and J. Noakes, Magnetic properties of Au₄X type ordered alloys, *J. Phys. Colloq.* **32**, C1-865 (1971).
- [10] C. Kittel, On the theory of ferromagnetic resonance absorption, *Phys. Rev.* **73**, 155 (1948).
- [11] X. Liu, Y. Sasaki, and J. K. Furdyna, Ferromagnetic resonance in Ga_{1-x}Mn_xAs: Effects of magnetic anisotropy, *Phys. Rev. B* **67**, 205204 (2003).
- [12] R. Skomski and J. M. D. Coey, Magnetic anisotropy—How much is enough for a permanent magnet? *Scr. Mater.* **112**, 3 (2016).
- [13] Y. He, T. Helm, I. Soldatov, S. Schneider, D. Pohl, A. K. Srivastava, A. K. Sharma, J. Kroder, W. Schnelle, R. Schaefer, B. Rellinghaus, G. H. Fecher, S. S. P. Parkin, and C. Felser, Nanoscale magnetic bubbles in Nd₂Fe₁₄B at room temperature, *Phys. Rev. B* **105**, 064426 (2022).
- [14] Y. He, S. Schneider, T. Helm, J. Gayles, D. Wolf, I. Soldatov, H. Borrmann, W. Schnelle, R. Schaefer, G. H. Fecher, B. Rellinghaus, and C. Felser, Topological Hall effect arising from the mesoscopic and microscopic non-coplanar magnetic structure in MnBi, *Acta Mater.* **226**, 117619 (2022).
- [15] Y. He, G. H. Fecher, C. Fu, Y. Pan, K. Manna, J. Kroder, A. Jha, X. Wang, Z. Hu, S. Agrestini, J. Herrero-Martín, M. Valvidares, Y. Skourski, W. Schnelle, P. Stamenov, H. Borrmann, L. H. Tjeng, R. Schaefer, S. S. P. Parkin, J. M. D. Coey, and C. Felser, A new highly anisotropic Rh-based heusler compound for magnetic recording, *Adv. Mater.* **32**, 2004331 (2020).
- [16] P. M. Oppeneer, I. Galanakis, P. James, O. Eriksson, and P. Ravindran, Theory of the anisotropic magneto-optical Kerr effect in artificial FeAu and MnAu and in XAu₄ (X= V, Cr, Mn) compounds, *J. Phys. Soc. Jpn.* **23**, 21 (1999).
- [17] I. Galanakis, M. Alouani, P. M. Oppeneer, H. Dreyssé, and O. Eriksson, Tuning the orbital moment in transition metal compounds using ligand states, *J. Phys.: Condens. Matter* **13**, 4553 (2001).
- [18] F. Gautier and Y. Petro, Anisotropie magnéto-cristalline des flms d'alliage Co_xPt_{1-x} étudiée par dichroïsme magnétique circulaire, 1999, https://biosoft-ipcms.fr/pdf/WG_PHD.pdf.
- [19] A. Rogalev, F. Wilhelm, N. Jaouen, J. Goulon, and J.-P. Kappler, X-ray magnetic circular dichroism: Historical perspective and recent highlights, in *Magnetism: A synchrotron Radiation Approach* (Springer, Berlin, 2006), (pp. 71–93).
- [20] P. Lynam, W. Proctor, S. M. Puri, and R. G. Scurlock, Hyperfine fields at ⁵⁵Mn in ordered Au-Mn alloys from low-temperature specific-heat measurements, *Phys. Rev. B* **2**, 2448 (1970).
- [21] S. Waki and S. Ogawa, Specific heat of CoS₂, *J. Phys. Soc. Jpn.* **32**, 284 (1972).
- [22] R. Caudron, R. Caplain, J.-J. Meunier, and P. Costa, Specific heat of dilute alloys of the transition metals in nickel, *Phys. Rev. B* **8**, 5247 (1973).
- [23] P. Hansen, C. Clausen, G. Much, M. Rosenkranz, and K. Witter, Magnetic and magneto-optical properties of rare-earth transition-metal alloys containing Gd, Tb, Fe, Co, *J. Appl. Phys.* **66**, 756 (1989).
- [24] *Magnetic Properties of Metals: D-element, Alloys, and Compounds*, edited by H. P. J. Wijn (Springer, New York, 1991).
- [25] J. Kübler, A. R. William, and C. B. Sommers, Formation and coupling of magnetic moments in Heusler alloys, *Phys. Rev. B* **28**, 1745 (1983).
- [26] M. A. Ruderman and C. Kittel, Indirect exchange coupling of nuclear magnetic moments by conduction electrons, *Phys. Rev.* **96**, 99 (1954).
- [27] E. Şaşıoğlu, L. M. Sandratskii, and P. Bruno, Role of conduction electrons in mediating exchange interactions in Mn-based Heusler alloys, *Phys. Rev. B* **77**, 064417 (2008).
- [28] M. Yessik, J. Noakes, and H. Sato, Magnetic properties of the pseudobinary alloys Au₄(Mn_{1-x}Cr_x), *J. Appl. Phys.* **41**, 1234 (1970).
- [29] M. A. AL-Jalali, Phenomenological analysis of the s-d exchange interaction in dilute Cu-Mn alloy at helium temperature, *Adv. Mater. Lett.* **5**, 14 (2014).
- [30] A. K. Majumdar, V. Oestreich, and D. Weschenfelder, Deviations from curie-weiss law in AuMn and AqMn spin-glasses, *Solid State Commun.* **45**, 907 (1983).
- [31] T. Hirone, T. Kaneko, and K. Kondo, The change of curie temperature of ordered Au₄Mn and of indium heusler alloy by hydrostatic pressure, *J. Phys. Soc. Jpn.* **18**, 65 (1963).
- [32] Y. He, J. Gayles, M. Yao, T. Helm, T. Reimann, V. N. Strocov, W. Schnelle, M. Nicklas, Y. Sun, G. H. Fecher, and C. Felser, Large linear non-saturating magnetoresistance and high mobility in ferromagnetic MnBi, *Nat. Commun.* **12**, 4576 (2021).
- [33] A. Neumann, L. Offernes, A. Kjekshus, and B. Klewe, The crystal structure of AuMnSn, *J. Alloys Compd.* **274**, 136 (1998).
- [34] S. N. Guin, Q. Xu, N. Kumar, H. Kung, S. Dufresne, C. Le, P. Vir, M. Michiardi, T. Pedersen, S. Gorovikov, S. Zhdanovich, K. Manna, G. Auffermann, W. Schnelle, J. Gooth, C. Shekhar, A. Damascelli, Y. Sun, and C. Felser, 2D-berry-curvature-driven large anomalous hall effect in layered topological nodal-line MnAlGe, *Adv. Mater.* **33**, 2006301 (2021).
- [35] K. V. Shanavas, Z. S. Popovic, and S. Satpathy, Theoretical model for Rashba spin-orbit interaction in d electrons, *Phys. Rev. B* **90**, 165108 (2014).
- [36] S. Mankovsky and H. Ebert, High-field magnetic susceptibility of Fe_{1-x}Co_x alloys, *Europhys. Lett.* **74**, 117 (2006).
- [37] H. Suzuki, J. Harada, T. Nakashima, and K. Adachi, Short-range ordering and ferromagnetic properties of disordered Au₄Mn Alloy, *Acta Crystallogr.* **A38**, 522 (1982).
- [38] Kaneko and M. Matsumoto, Anomalous thermal expansion and specific heat of the ferromagnetic compound Au₄Mn, *J. Phys. Soc. Jpn.* **27**, 1141 (1969).
- [39] T. Goto, K. Fukamichi, T. Sakakibara, and H. Komatsu, Itinerant electron metamagnetism in YCo₂, *Solid State Commun.* **72**, 945 (1989).